The multimodal integration of EEG, MEG and functional MRI in the study of human brain activity

Fabio Babiloni[1,2]

1 *Dep. Human Physiology and Pharmacology, University "La Sapienza", Rome, Italy*
2 *IRCCS "Fondazione Santa Lucia", Rome, Italy*

Introduction

Nowadays, it is well understood that brain activity generates a variable electromagnetic field that can be detected quite accurately by using scalp electrodes as well as by superconductive magnetic sensors. Electroencephalography (EEG) and magnetoencephalography (MEG) are therefore useful techniques for the study of brain dynamics and functional cortical connectivity, because of their high temporal resolution (milliseconds [1,2]). Electroencephalography reflects the activity of cortical generators oriented both in tangential and radial way with respect to the scalp surface, whereas MEG reflects mainly the activity of the cortical generators oriented tangentially with respect to the magnetic sensors. However, the different electrical conductivity of the brain, skull and scalp markedly blurs the EEG potential distributions and makes the localization of the underlying cortical generators through this technique a problematic issue. To overcome this problem, high-resolution EEG (HR-EEG) technology was introduced during the last decade and was shown to greatly improve the spatial resolution of the conventional EEG [2–4]. Such technology included (i) the use of realistic head models obtained from sequential magnetic resonance imaging (MRI) of the subject's head, to mathematically model the propagation of the potential from the cortex to the scalp sensors; (ii) the sampling of the spatial distribution of scalp potential with a high number of surface electrodes (64–128); (iii) the use of mathematic Laplacian (SL) operators to improve the spatial details of the recorded scalp potential distribution; (iv) the use of an accurate model for the cortical sources that typically includes 3000–5000 current dipoles.
However, the spatial resolution of the HR-EEG/MEG techniques is fundamentally limited by the inter-sensor distances and by the fundamental laws of electromagnetism [1]. Despite the lack of spatial resolution for these techniques, neural sources can be localized from HR-EEG or MEG data by making a priori hypotheses on their number and extension. When a known number of cortical sources (i.e. short-latency evoked potentials) generate the neuronal activity, the location and strength of these sources can be reliably estimated by the dipole localization technique [5]. However, with the exception of the early processing of sensory responses, event-related cortical responses include a distributed network of several and unknown areas. When the distributed cortical network is supposed to be active, neural sources could be modeled by linear inverse estimation [6,7]. This approach implies the use of both thousands of equivalent current dipoles as a source model and realistic head models, reconstructed from magnetic resonance images, as a volume conductor medium. The use of geometrical constraints can generally reduce the solution space (i.e. the set of all possible combinations of the cortical dipoles strengths). For example, the dipoles can be disposed along the reconstruction of cortical surface with a direction perpendicular to the local surface. An additional constraint is to force the dipoles to explain the recorded data with a minimum or a low amount of energy (minimum norm solutions [6,8]). In addition, the use of a priori

information from other neuro-imaging techniques having high spatial resolution, like functional magnetic resonance imaging (fMRI), has been suggested to improve the localization of sources from HR-EEG/MEG data [8,9]. In fact, human neocortical processes involve temporal and spatial scales spanning several orders of magnitude, from the rapidly shifting somato-sensory processes characterized by a temporal scale of milliseconds and a spatial scale of a few square millimeters to the memory processes involving periods of seconds and spatial scale of square centimeters. Information about the brain activity can be obtained by measuring different physical variables linked to the brain processes, such as the increase in consumption of oxygen by the neural tissues or the variation of the electric potential over the scalp surface. It is worth noting that all these variables have their own spatial and temporal resolution. The different neuro-imaging techniques are thus confined to the spatio-temporal resolution offered by the measured variables. Today, no neuro-imaging method provides at the same time for a spatial resolution on a millimeter scale and a temporal resolution on a millisecond scale. As a consequence of the previous statement, the functional brain images obtained with the various techniques at our disposal (fMRI, HR-EEG, MEG) are like the pieces of a puzzle, the "neuro-imaging puzzle", that we have to put together to retrieve a unique picture of the underlying brain activity. Hence, it is of interest to study the possibility of integrate the information offered by the different physiological variables related to the brain functions in a unique mathematical context. This operation is called the "multimodal integration" of variables X and Y, where the X variable typically has particularly appealing spatial resolution property (millimeter scale) and the Y variable has particularly attractive temporal properties (millisecond scale). Nevertheless, the issue of several temporal and spatial domains is critical in the study of brain functions, since different properties could become observable, depending on the spatiotemporal scales at which the brain processes are measured. The rationale of the multimodal approach based on fMRI, MEG and HR-EEG data to locate brain activity is that neural activity generating EEG potentials or MEG fields increases glucose and oxygen demands [10]. This results in an increase in the local hemodynamic response that can be measured by fMRI [11,12]. Overall, such a correlation between electrical and hemodynamic concomitants provides the basis for a spatial correspondence between fMRI responses and HR-EEG/MEG source activity. Furthermore, numerical simulations have shown that the use of fMRI priors increases the quality of the cortical current estimations for both HR-EEG and MEG recordings [9,13,14].
In the following, we first present the mathematical principle of the multimodal integration of HR-EEG with MEG data. Then, we show how to integrate mathematically HR-EEG/MEG data with fMRI data. Besides these methodologies, we present some practical applications for the localization of sources responsible for intentional simple movements executed by healthy subjects.

Cortical activity estimation from non invasive EEG and MEG measurements

The Head and the Source Models

Let us assume an EEG recording performed with a set of M electrodes disposed on the scalp surface. In the following, we indicate with **b** the vector of M electrical measurements recorded from the scalp. In order to perform the estimation of the cortical activity we also need a model of the head volume conductor. This model is used to approximate the propagation of the potential from the modeled neural generators to the measurement sensors. The head model can be of spherical or elliptical shape or can recall the realistic head shape. Since we have to estimate the source activity from non-invasive EEG measurements, we need a mathematical model for the neural sources. In the analysis of EEG and MEG, the largely used mathematical model for the neural source is the current

dipole. Such model is largely used in literature since approximates very well the activity of relatively small patches of the cortical tissue. In this particular context, we used many current dipoles located in the brain along the entire cerebral volume or along its cortical surface. If we would like to model the entire brain volume, we had to divide it in voxels and then placing a triplet of orthogonal current unitary dipoles at each voxel position. Another source model takes into account only the cortical geometry, to constraint the dipoles to lie orthogonal to the modeled cortical surface. In the following, we deal with the problem of source estimation by using a representation of the cortical surface, and we use a set of dipoles disposed along such surface as source model (see Fig. 1). However, all the mathematical formulas presented here still hold also in the case in which the neuronal space is divided in voxels, attempting to model also the subcortical structures.
Each dipole placed inside the volume conductor model of the head has a unitary strength and different direction, according to the local cortical geometry or to the adopted reference coordinate system. There is no limitation for the number of sources placed inside the head model, which depends on the modeling capabilities of the used computational system. In the following, we indicate with N the number of dipoles whose strength is to be estimated from the M-dimensional measurement vector **b**. The typical values for N are between 1000 and 7000, while the values for M are in the range 64-256. We indicate as x the n-dimensional vector of the unknown current strengths for the dipoles.

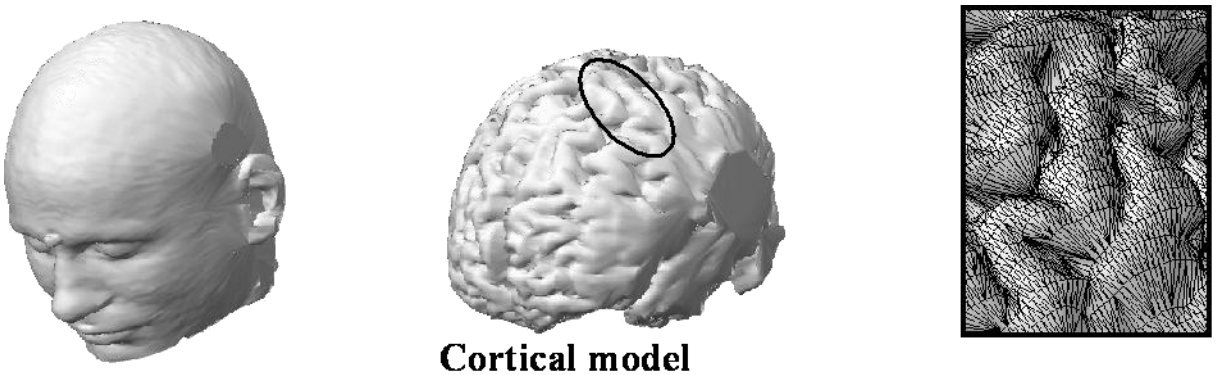

Fig. 1 Realistic head model for linear inverse source estimation. Note the particular showing the hand area tessellated with triangles (right figure). At the center of each triangle, a dipole with unitary strength and perpendicular to the triangle was posed.

The Linear Inverse Problem

In the estimation of neuronal activity from non-invasive measurements, we have to use a mathematical model for the description of the propagation of the potential distribution from each modeled sources to the sensors positions. In other words, we have to compute the potential distribution occurring on the set of the M sensors over the head model due to the *i-th* unitary dipole placed at the *i-th* cortical location. Such predictions can be made with the aid of analytical or boundary-element formulations, depending on the shape of the head model used. While the equation for the potential distribution for a three-layered spherical head model can be found in literature, in **appendix I** are reported the equations that compute the potential value due to a dipole inside a realistic head model over a point located on the scalp surface. Such equations are for the electric case, while those in **appendix II** are for the magnetic case.
In the following, we indicate as **Ai** the potential distribution over the M sensors due to the unitary *i-th* cortical dipole**.** The collection of all the M-dimensional vectors **Ai**, (i = 1,…, N) describes how

each dipole generates the potential distribution over the head model. This collection is called the lead field matrix **A**.
With the definitions provided above, we can say that the estimate of the strength of the modeled dipolar source strength **x** from the non invasive set of measurement **b,** is obtained by solving the following linear system:

$$Ax = b \quad \textbf{(1)}$$

where **A** is the M x N lead field matrix, **x** is the N-dimensional array of the unknowns cortical strengths and **b** is the M-dimensional vector of the instantaneous (electrical or magnetic) measurements. This is a strongly underdetermined linear system, in which the number of the unknown variables (i.e. the dimension of the vector **x),** is greater than the number of measurement **b** of about one order of magnitude. In this case, from the linear algebra we note that there are infinite solutions for the vector of dipole strengths **x**. All these solutions explain in the same way the data vector **b**. Furthermore, the linear system is ill conditioned as results of the substantial equivalence of the several columns of the electromagnetic lead field matrix **A**. In fact, we know that each column of the lead field matrix arise from the potential distribution generated by the dipolar sources that are located in similar position and orientation along the used cortical model. Regularizing the inverse problem consists in attenuating the oscillatory modes generated by vectors associated with the smallest singular values of the lead field matrix **A**, introducing supplementary and a priori information on the sources to be estimated. In the following, we characterize with the term "solution space" the space in which the "best" current strength solution **x** will be found. The "measurement space" is the vectorial space in which the vector **b** of the gathered data is considered. The solution of the linear problem **Ax = b** with the variation approach is based on the idea of selecting metrics from the solution space and the measurement space, respectively. These two metrics are characterized by symmetric matrices and express our idea of closeness in the same spaces. With this approach, the minimization function is composed of two terms, one that evaluates how well the solution explains the data, and the other that measures the closeness of the solution to an a priori selected.
The formulation of the problem expressed in the eq.1 now becomes:

$$\xi = \text{argmin} \left(\| (Ax-b) \|_{Wd}^2 + \lambda^2 \| x \|_{Wx}^2 \right) \quad \textbf{(2)}$$

where the matrices **Wd** and **Wx** are associated with the the metrics of the measurement and source space, respectively, and **λ** is the Lagrangian parameter. The source estimate **ξ** was hence the source distribution that between the infinite possible solutions to the undetermined problem described in the equation 2 explains the EEG data with a minimum amount of energy (weighted minimum norm solution). By setting the matrices **Wd** and **Wx** to the identity, the minimum norm estimation was obtained.
The solution of the problem described in eq. 2 has the following the form:

$$\xi = Gb \quad \textbf{(3)}$$

where under the hypothesis that the metric **Wx** and **Wd** are invertible the pseudo-inverse matrix **G** is given by

$$G = W_x^{-1} A' (A W_x^{-1} A' + \lambda W_d^{-1})^{-1} \quad \textbf{(4)}$$

Hamalainen and Ilmoniem proposed the estimation of the cortical activity with the minimum norm solution in 1984 [8]. However, it was recognized that in this particular application, the solutions

obtained with the minimum norm constraints were biased toward those dipoles that are located nearest to the sensors. In fact, there is a dependence of the distance in the law of potential (and magnetic field) generation and this dependence tends to increase the activity of the more superficial dipoles while depress the activity of the dipoles far from the sensors. The solution to this bias was obtained by taking into account a compensation factor, for each used dipole, that equalized the visibility of the dipole from the sensors. This technique, called column norm normalization was used in the linear inverse problem by Pascual-Marqui [15] and then adopted largely by the scientist in this field. With the column norm normalization, a diagonal NxN matrix **W** was formed, whose generic *i-th* term on the diagonal is equal to:

$$W_{ii} = ||Ai||^{-2} \quad \textbf{(5)}$$

representing the L2-norm of the *i-th* column of the lead field matrix **A**. In this way, dipoles near to the sensors (with a large || **Ai**.||) will be depressed in the solution of eq.2, since their activations are not convenient from the point of view of the functional cost. In fact, dipoles with low visibility from the sensors (with a low ||**Ai**||) have an associate cost function convenient to use. The use of this **Wx** matrix in the source estimation is known as weighted minimum norm solution [16].
Another question of interest in the solution of linear inverse problem is the setting of the Lagrangian parameter **λ** that regulates the presence of the a priori information inside the solution of the problem. How it is possible to set such parameter in an "optimal" way?
An optimal regularization of the linear system described in eq.2 was obtained through the Tikhonov and L-curve approach [17]. This curve plots the residual norm versus the solution norm at different values of the regularization parameter lambda. It is worth of notice that the optimal regularization value can be selected automatically. In fact, this value is located at the "corner" of the L-curve plot. Other criteria for choosing the value of lambda are for instance the Generalized Cross Validation (GCV) or the CRESO method together with the zero-crossing method and the relative minimal product.

Multimodal Integration of EEG and MEG data

At a first look, the attempt to integrate the EEG and MEG data in order to increase the quality of the source reconstruction fails when we consider that the units of the electrical and magnetic fields differ. How we can fuse these data together? One possible answer is to transform the measurements produced by the electric and magnetic sensors in terms of standard deviations of measurement noise. In this way, both the electrical and magnetic values are transformed and then reported on a common scale.
In this context, the estimation of the covariance matrix of the electrical and the magnetic noise assumes a particular emphasis. The estimation of such matrices requires the recording of several single sweeps of EEG and MEG data, and the possibility to determine a segment of the recorded data in which no task-related activity is present. Then, the maximum likelihood estimates for the covariance matrices of the noise electrical **Ne** and magnetic **Nm** matrices have to be computed on all the sweeps recorded for the period of interest. With the use of these matrices, we can produce the block covariance matrix of the electromagnetic measurement, called **S** by **S** = (**Ne Nm**).
The forward solution specifying the potential scalp field due to an arbitrary dipole source configuration was computed according to the following linear system:

$$\begin{bmatrix} E \\ B \end{bmatrix} [x] = \begin{bmatrix} v \\ m \end{bmatrix} \quad \textbf{(6)}$$

where ***E*** is the electric lead field matrix obtained by the boundary element technique for the realistic MR-constructed head model and ***B*** is the magnetic lead field matrix obtained for the same head model. ***x*** is the array of the unknown cortical dipole strengths, ***v*** is the array of the recorded potential values and ***m*** is the array of magnetic values. The lead field matrix ***E*** and the array ***v*** were referenced consistently. In order to scale the EEG and MEG data, the rows of the lead field matrix **E** and **B** was first normalized by the rows norm [18]. This scaling is applied in the same way on the electrical and magnetic measurements arrays, ***v*** and ***m***. After row normalization, the linear system can be restated as:

$$\underline{A}x = \underline{b} \qquad \textbf{(7)}$$

where **A** is the matrix composed of the normalized electric and magnetic lead fields, and **b** is the normalized measurement array of EEG and MEG data (***v*** and ***m***), respectively.
As already noted before, the general formulation of the linear inverse problem based on this assumption is:

$$\underline{\xi} = \text{argmin}\left(\| (\underline{A}x-\underline{b})\|_{\underline{Wd}}^{2} + \lambda^{2} \| x\|_{\underline{Wx}}^{2}\right) \qquad \textbf{(8)}$$

where **Wd** is now equal to the covariance matrix **S** of the noise of the normalized EEG and MEG sensors, while **Wx** is the matrix that regulates how each EEG or MEG sensor is influenced by dipoles located at different depths into the source model. The covariance matrix **S** was derived from the normalized EEG and MEG data by means of the maximum likelihood estimation as described before. It is essential that the estimate of **S** have to be performed on both EEG and MEG data with maximum background electromagnetic noise (i.e., no event-related electromagnetic signal). The matrix **Wx** is a diagonal matrix in which the *i-th* element is equal to the norm of the *i-th* column of the normalized lead field matrix **A**. As said before, an optimal regularization of the linear system **Ax** = **b** was obtained by the L-curve approach [17] that plots the residual norm versus the solution norm at different values of the regularization parameter lambda.
In figure 2, we show a representative result obtained from the linear inverse estimates of EEG, MEG and combined EEG-MEG data. The recordings were performed during the voluntary movement of the right middle finger.

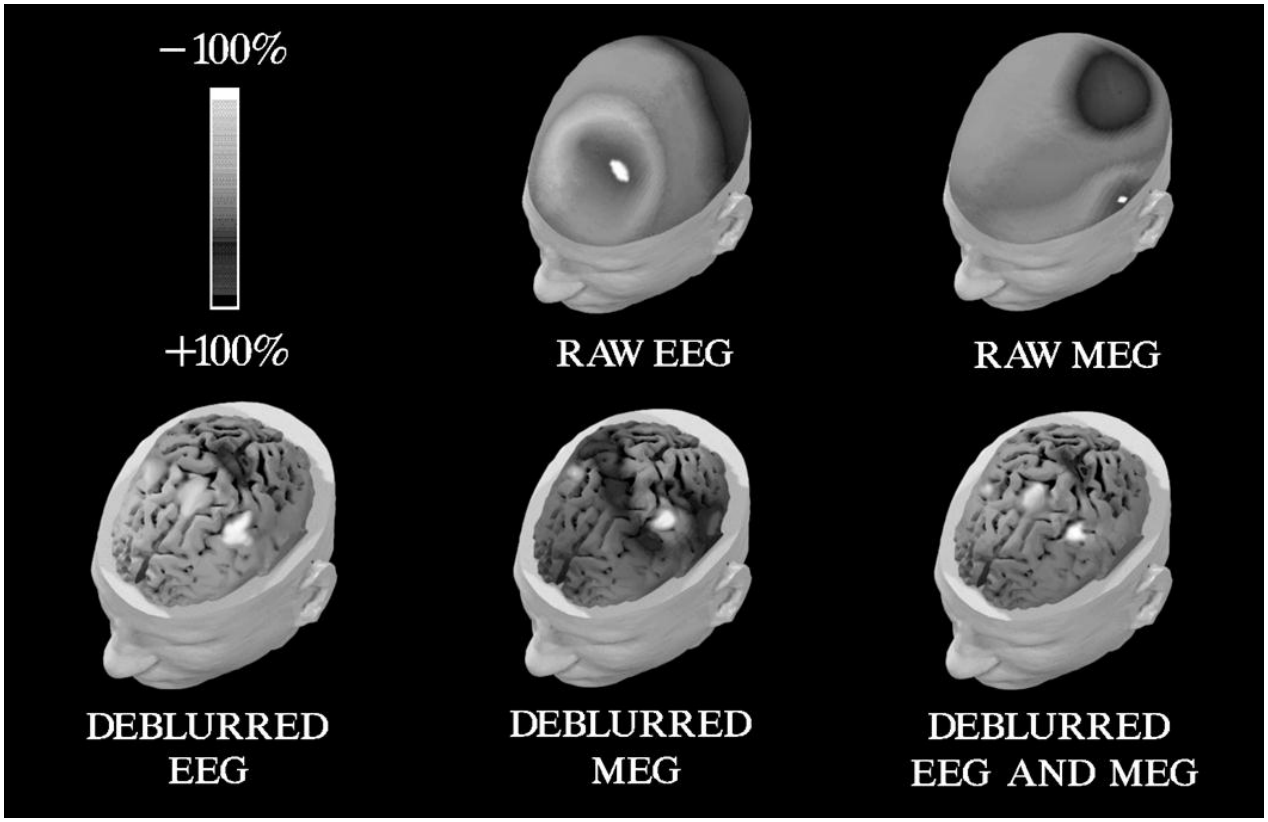

Fig. 2. Amplitude grey scale 3-D maps showing linear inverse estimates of electroencephalographic (EEG), magnetoencephalographic (MEG), and combined EEG-MEG data recorded (128-50 channels, respectively) from a subject about 110 msec after the onset of electromyographic response accompanying a voluntary brisk right middle finger extension. The original movement-related EEG and MEG activity is also shown as a reference. Linear inverse estimates were mapped as electric fields forwarded over the dura mater compartment of the realistic magnetic resonance-constructed subject's head model. Percent gray scale (256 hues) is normalized with reference to the maximum amplitude calculated for each map. Maximum negativity (-100%) is coded in white and maximum positivity (+100%) in black.

Integration of EEG/MEG and fMRI data

In this section, a proposal for the use of fMRI constraints in the source estimate by the linear inverse problem is described. In the following, we assume to deal with the issue of integrating EEG and fMRI data, but we would like to note that a similar approach could be produced also for the fusion of the MEG with fMRI data. The methodology for the combination of all the modalities together (i.e. EEG, MEG and fMRI) for the source estimation will be the union of the techniques presented here and in the previous section.

The Common Head Model

One fundamental issue in the integration of the fMRI with the EEG data is the use of a common geometrical framework to register the volume conductor of the head model and the activated voxels deriving from the fMRI images. To do that, the fMRI images have to be first co-registered with the anatomic images of the subject's head, which were obtained by the acquisition of T1-weighted

conventional spin-echo-axial-oblique sequence. The sequential MR images of the analyzed subject constituted also the base for the construction of the volume conductor of the head model to be used in the EEG analysis. In this context, the structure for the scalp, skull and dura-mater have to be recognized from the MR images by automatic or semi-automatic segmentation procedure.
Once the different structures for scalp, skull and dura-mater have been recognized and tessellated, the use of the boundary element modeling technique allows computing the potential distribution over the sensors generated by a dipole inside the brain. A brief description of the analysis is described in **Appendix I**. Once the common geometrical reference for the head for both EEG and fMRI measurements has been established, the fusion of the information from the activated brain voxels during EEG data acquisition can be addressed.

The Percentage Change Hemodynamic Responses

In the fMRI analysis, several methods to quantify the brain hemodynamical response during a particular task have been developed. Here we recall the Statistical Parametric Mapping (SPM) introduced at the early 90 by K.J. Friston, or methods relying on the use of statistical Bonferroni-corrected t-test, or those based on the Kolmogorov-Smirnof tests. In principle, the issue of the integration between EEG and fMRI does not depend on the particular method used for the fMRI analysis. However, in order to illustrate the technique, in the following we analyze the case in which a particular fMRI quantification technique has been employed, called Percent Change technique. This measure quantifies the percentage increase of the fMRI signal during the task performance with respect to a resting state. The visualization of the voxels distribution in the brain space that are statistically increased during the task condition with respect the rest is called the PC (percent change) map. The difference between the mean rest and movement-related signal intensity is generally calculated voxel-by-voxel. The rest-related fMRI signal intensity is obtained by averaging the pre-movement and recovery fMRI. The Bonferroni-corrected Student's t-test is also used to minimize the alpha inflation effects due to multiple statistical voxel-by-voxel comparisons (Type I error; $p<0.05$). Voxels with a statistically significant PC activation have to be projected onto the modeled cortical surface. PC values of the statistically activated voxels assigned to a certain cortical triangle are summed as a measure of the movement-related cortical activation. This measure corresponded to the αi value that must be used as weighting function in the successive linear inverse minimization procedure.

EEG linear inverse estimation

The forward solution specifying the potential scalp field due to an arbitrary dipole source configuration is computed according to the linear system described in eq. 2. The lead field matrices **A** and the data **b** array have to be referenced consistently. To obtain a unique solution of the linear system (eq. 1), the variational problem for the sources **x** was posed as described in eq. 8. The solution of the variational problem depended on adequacy of the data and source space metrics. The metric for the data space was obtained by the use of statistics about the residual $\mathbf{n} = \mathbf{Ax} - \mathbf{b}$. The metric for the source space was based on the norm of the residual vector **n.** The Mahalanobis metric for the data space has to be preferred here since it permitted to take into account easily information from combined EEG and MEG data (see previous section). The metric for the source space has to take into account the normalization of the lead field matrix **A** to balance the much more visibility of the superficial cortical sources from the EEG data with respect to the deepest ones. Furthermore, in the source metric we would like to insert the a priori information that comes from the fMRI-activated voxels. To do that, we use the percentage intensity values (α) of the integrated fMRIs. The metric for the source space is then formed by a diagonal matrix **W**, the *i-th* term of which was:

$$Wii = ||Ai||^2 \, g\square(\alpha_i)^{-2} \quad \textbf{(9)}$$

where $||\mathbf{A_i}||$ is the norm of the i-th column of the lead field matrix A and $\mathbf{g\square(\alpha_i)}$ is a function of the statistically significant percentage increase of the fMRI signal assigned to the i-th dipole of the modeled source space. The $\mathbf{g\square(\alpha_i)}$ function is expressed as:

$$g(\alpha_i) = 1 + K\,\alpha_i\,, \qquad \alpha_i \geq 0; \quad \textbf{(10)}$$

where the factor **K** tunes the fMRI solutions in the source space for the time varying electromagnetic component **b**. By inspecting eq. 9, high **K** values (i.e., $\mathbf{K}\,\boldsymbol{\alpha_i} \approx 10$) produce a space norm **W**, which is roughly one order of magnitude lower than the one obtained by taking into account the only column normalization. On the other hand, low **K** values (i.e., $\mathbf{K}\,\boldsymbol{\alpha_i} << 1$) result in a **W** value roughly proportional to the squared column norm, which completely disregards the fMRI solution (i.e., 0% fMRI solution or 100% EEG solution).
With the used metric, the pseudo-inverse matrix **G** now depends on the **K** values. The problem with this optimal regulation of the **K** value is the computational effort that can be remarkable when realistic source models with thousands of dipoles are used. However, the mean computational power available on personal computers doubles each 1.5 year. Hence, the actual computational effort to compute the EEG and fMRI integration cannot represent a serious problem in the next years. As a last statement of this review, it is possible to note that integration of EEG, MEG and fMRI data can be possible by solving the linear inverse problem depicted in the eq. 8 with **Wd** equals to the covariance matrix of the electromagnetic noise and with **Wx** equals to that described in eq. 9.
In figure 3, we show a representative result obtained from HR-EEG data and HR-EEG combined with fMRI data. The recordings were performed during the voluntary movement of the right middle finger.

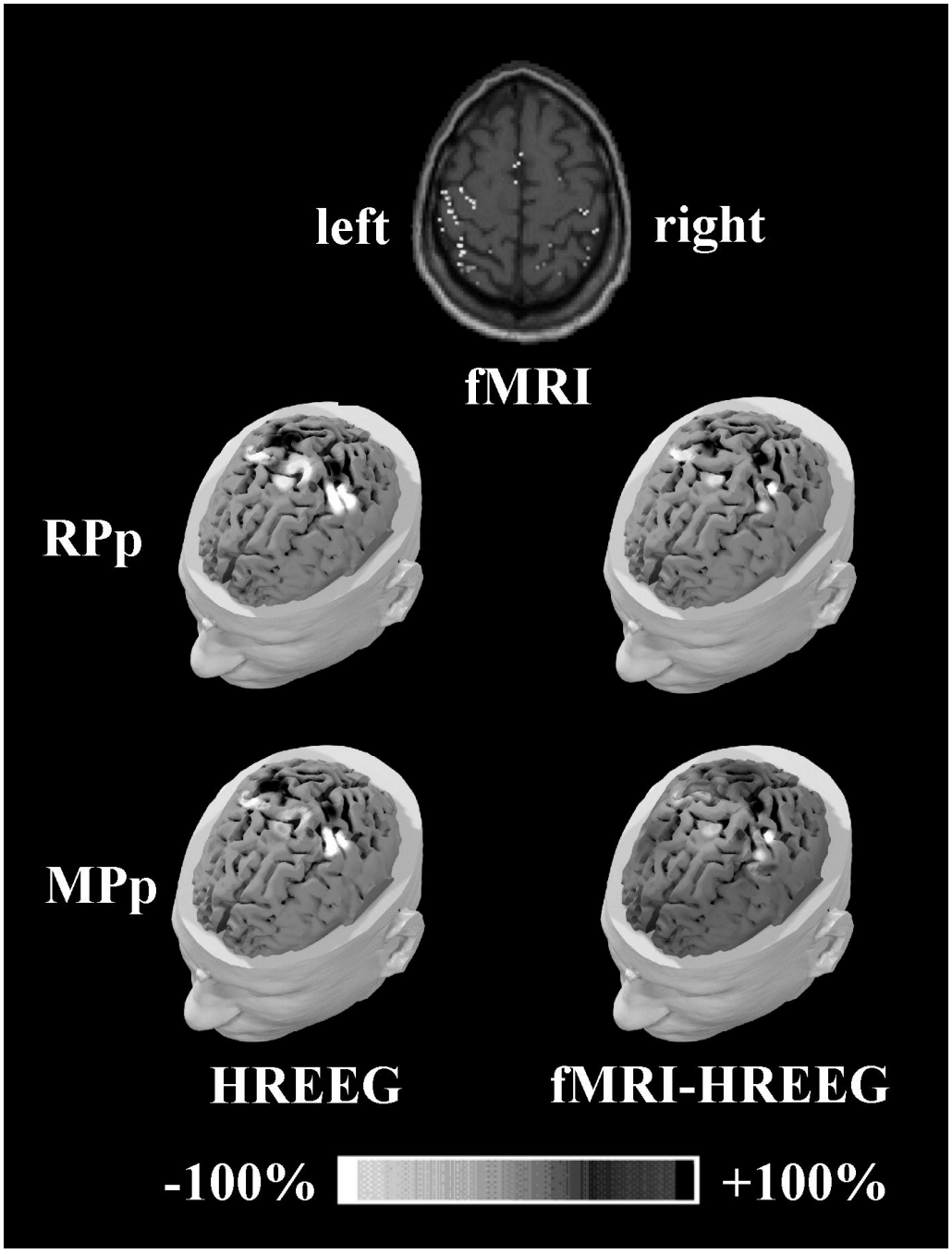

Fig.3 Amplitude grey scale 3-D maps showing linear inverse estimates from high resolution electroencephalographic (HREEG) and combined functional magnetic resonance image (fMRI)-HREEG data computed from a subject about 50 msec before (readiness potential peak, RPp) and 20 msec after (motor potential peak, MPp) the onset of the electromyographic activity associated with self-paced right middle finger movements. A representative axial PC map of statistically significant ($p<0.05$) fMRI signal intensity is also shown as a reference (top). The linear inverse estimate of HREEG and combined fMRI-HREEG data were mapped as electric fields forwarded over the dura mater compartment of a realistic MRI-constructed subject's head model. In fMRI data statistically activated voxels are represented in white. Percent grey scale (256 hues) of HREEG and combined fMRI-HREEG data is normalized with reference to the maximum amplitude calculated for each map. Maximum negativity (-100%) is coded in white and maximum positivity (+100%) in black.

Appendix I. Electrical forward solution for a realistic head model

Let a head model be constituted by electrically homogeneous and isotropic compartments simulating scalp, skull, and dura-mater. The forward solution specifying the potential distribution (V) on these compartments S_k (k = 1,...3) due to a dipole is given by the Fredholm integral equation of the second kind:

$$\left(\sigma_i^- + \sigma_i^+\right)V\left(\vec{r}\right) = 2V_0\left(\vec{r}\right) + \frac{1}{2\pi}\sum_{j=1}^{m}\left(\sigma_j^- - \sigma_j^+\right)\int_{S_j} V\left(\vec{r}'\right)d\Omega_{\vec{r}}\left(\vec{r}'\right) \qquad \textbf{(A. 1)}$$

With

$$d\Omega_{\vec{r}}\left(\vec{r}'\right) = \frac{\vec{r}'-\vec{r}}{\left|\vec{r}'-\vec{r}\right|^3}\,d\vec{S}_j\left(\vec{r}'\right) \qquad \textbf{(A. 2)}$$

where (i) $V_0\left(\vec{r}\right)$ is the potential due to a dipole located in an infinite homogeneous medium; (ii) σ_j^- is the conductivity inside the surface S_j of the multi-compartment head model; (iii) σ_j^+ is the conductivity outside the surface S_j; (iv) m is the total number of compartments within the head model; and (v) $d\Omega_{\vec{r}}\left(\vec{r}'\right)$ is the solid angle subtended by the surface element dS located in $\vec{r}$ (point of observation $\vec{r}'$). A numerical solution of the Fredholm integral equation can be obtained by decomposing the surfaces S_k (k = 1,...3) into triangle panels and by using boundary element techniques. With the boundary-element techniques, a discrete version of the Fredholm integral equation is given by

$$v = g + \Omega\, v \qquad \textbf{(A. 3)}$$

where the elements of matrix **Ω,** vector **v**, and vector **g** are defined as follows: (i) vi is the potential value in the center of mass of the i-th triangle; (ii) gi is the potential value generated by a source in the center of mass of the i-th triangle; and (iii) Ωij is the matrix element proportional to the solid angle subtended by the j-th triangle at the center of mass of the *i-th* triangle. The numerical solution of the Fredholm integral equation can be improved using the deflation procedure. The linear system of equation A.3 is singular since the potential distribution generated on the scalp compartment by an equivalent dipole is determined up to a constant**.** This singularity can be removed by using a deflation procedure that yields the potential distribution (V) on the compartment surfaces S_k (k = 1,...3).

Appendix II. Magnetic forward solution

The magnetic field of a current dipole in a piecewise homogenous conducting medium is given by

$$B = B_0 + \frac{\mu_0}{4\pi}\sum_{j=1}^{m}\left(\sigma_j^+ - \sigma_j^-\right)\int_{S_j} V(\vec{r})\frac{\vec{n}\times(\vec{r}-\vec{r}')}{\left|\vec{r}-\vec{r}'\right|^3}dr' \qquad \textbf{(A. 4)}$$

where (i) B_0 is the field of the current dipole in the free space with each surface integral extending to an interface between homogeneously conducting media; (ii) n is a unit vector orthogonal to the surface S_j; and (iii) the summation index j runs over the surfaces. The surface integrals take into account the effects of volume currents. Notice that these currents are equivalent to layers of current dipoles orthogonal to the interfaces, with dipole moment per unit area $V(\sigma^+-\sigma^-)$. The magnetic lead field matrix was calculated by adding, for each dipole, the free space term and the corresponding volume current term. Since a boundary element model was used, the volume currents were modeled by an array of fictitious dipoles, located at the centroids of each triangle of the reconstructed surfaces, with moment $V(\sigma^+-\sigma^-)$ times the triangle area.

References

[1] Nunez P. Electric fields of the brain. New York7 Oxford University Press; 1981.

[2] Nunez PL. Neocortical dynamics and human EEG rhythms. New York, Oxford University Press; 1995.

[3] Gevins A, Brickett P, Reutter B, Desmond J. Seeing through the skull: advanced EEGs use MRIs to accurately measure cortical activity from the scalp. Brain Topogr 1991;4:125 – 31.

[4] Gevins A, Le J, Leong H, McEvoy LK, Smith ME. Deblurring. J Clin Neurophysiol 1999;16(3):204– 13.

[5] Scherg M, von Cramon D, Elton M. Brain-stem auditory-evoked potentials in post-comatose patients after severe closed head trauma. J Neurol 1984;231(1):1– 5.

[6] Dale AM, Sereno M. Improved localization of cortical activity by combining EEG and MEG with MRI cortical surface reconstruction: a linear approach. J Cogn Neurosci 1993;5:162 – 76.

[7] Dale A, Liu A, Fischl B, Buckner R, Belliveau JW, Lewine J, et al. Dynamic statistical parametric mapping: combining fMRI and MEG for high-resolution imaging of cortical activity. Neuron 2000;26: 55– 67.

[8] H7m7l7inen M, Ilmoniemi R. Interpreting measured magnetic field of the brain: estimates of the current distributions. Tech Rep TKKF- A559. Espoo (Finland): Helsinki University of Technology; 1984.

[9] Liu AK, Belliveau JW, Dale AM. Spatiotemporal imaging of human brain activity using functional MRI constrained magnetoencephalography data: Monte Carlo simulations. Proc Natl Acad Sci U S A 1998; 95(15):8945– 50.

[10] Magistretti PJ, Pellerin L, Rothman DL, Shulman RG. Energy on demand. Science 1999;283(5401):496– 7.

[11] Grinvald A, Lieke E, Frostig RD, Gilbert CD, Wiesel TN. Functional architecture of cortex revealed by optical imaging of intrinsic signals. Nature 1986;324(6095):361–4.

[12] Puce A, Allison T, Spencer SS, Spencer DD, McCarthy G. Comparison of cortical activation evoked by faces measured by intracranial field potentials and functional MRI: two case studies. Hum Brain Mapp 1997;5(4):298 –305.

[13] Liu AK. Spatiotemporal brain imaging. PhD dissertation. Cambridge (Mass): Massachusetts Institute of Technology; 2000.

[14] Babiloni F, Babiloni C, Carducci F, Romani GL, Rossini PM , Angelone LM and Cincotti F, Multimodal Integration of High Resolution EEG and Functional Magnetic Resonance Imaging Data: a Simulation Study, *Neuroimage*, 2003,*;19(1):1-15.*

[15] Pascual-Marqui, R.D. (1995) Reply to comments by Hamalainen, Ilmoniemi and Nunez. In ISBET Newsletter N.6, December 1995. Ed: W. Skrandies., 16-28.

[16] Grave de Peralta, R.., Hauk, O., Gonzalez Andino, S., Vogt, H., and Michel, C.M., 1997, Linear inverse solution with optimal resolution kernels applied to the electromagnetic tomography, Human Brain Mapping **5**, 454-67.

[17] Hansen PC. Analysis of discrete ill-posed problems by means of the L-curve. SIAM Rev 1992;34:561– 80.

[18] Phillips, J.W., Leahy, R. and Mosher, J.C., 1997, MEG-based imaging of focal neuronal current sources, IEEE Trans. Med. Imag., vol. 16., n.3, pp. 338-348.